

SQUID Attack!

Julie Bowles
IRM

Modern rock- and paleo-magnetism have come to strongly rely on extremely sensitive measurements provided by the superconducting quantum interference device (SQUID). At the IRM, both of our 2G magnetometers and both Magnetic Properties Measurement Systems (MPMS) operate using SQUIDs. Despite its pervasiveness in magnetometer systems of various sizes and shapes, a general understanding of how SQUIDs work is not widespread. For many people (including the author), the ten-armed variety (Fig. 1) is far more familiar and comprehensible (not to mention tasty). This short article aims to shine a little light on the subject. (Or, if you prefer, slather on a little garlic-butter sauce to make it more palatable.) Several excellent reviews of SQUID devices have been provided by others (Gallop and Petley, 1976; Goree and Fuller, 1976; Petley, 1980; Clarke, 1994), and the more rigorous mathematical details are left to them. Neither is this piece intended as a detailed description of electronics. Hopefully what will be provided is simply a little deeper understanding of what is going on when you hit that “measure” button on your instrument.

We will start with a review of the theoretical underpinnings of SQUID devices, and then move to descriptions of both the DC and RF SQUID and how they are operated as flux measurement devices.

The Theory

We begin our journey toward SQUID comprehension by starting with the basics, the SQU in SQUID: superconductivity and the quantization of magnetic flux.

Superconductivity. Certain metals when cooled below a **critical temperature** (T_c) are able to conduct current with zero resistance or voltage, an observation that earned the Nobel Prize for Dutch physicist Heike Kamerlingh Onnes in 1911. It wasn't until 1957, however, with the description of BSC theory (Bardeen, Cooper, and Schrieffer, 1957) and the so-called Cooper pair, that the phenomenon was understood. In normal material, resistivity results from the interaction of electrons with the crystal lattice. In superconducting materials at $T < T_c$, lattice vibrations are suppressed and two electrons of

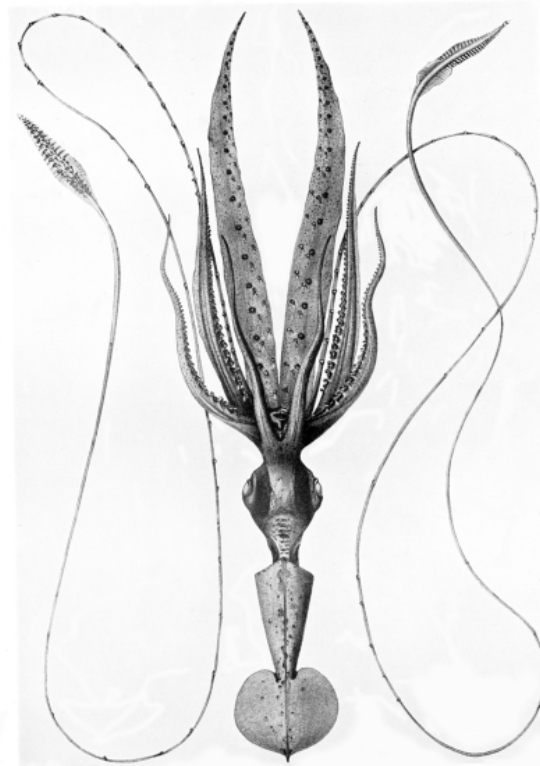


Figure 1. *Chroteuthis veranyi*, by Georg Pfeffer, *Die Cephalopoden der Plankton-Expedition, 1912*.

opposite spin and momentum are weakly bound together as a Cooper pair and move through the lattice with zero resistance. In addition to a critical temperature, there also exist a **critical field** (B_c) and a **critical current** (I_c) above which a superconductor reverts to the normal state and develops resistance. The critical current is an important feature of the SQUID, as we will see below.

Flux quantization. In a closed loop of superconducting material, the flux threading the loop can only take on discrete values. This can be understood by considering that within a superconductor all the electrons (Cooper pairs) have the same quantum wave function, and around any closed path the phase (θ) of this function must be an integral number such that

$$\oint d\theta = n2\pi \quad \text{Eq. 1}$$

(e.g. Gallop and Petley, 1976; Kleiner and Koelle, 2004). If the phase were to vary by a fraction of $n2\pi$, then the wave function would not be unique. In terms of angular momentum, all the Cooper pairs have the same angular momentum, which can only take on a discrete set of states according to the Bohr quantization rule (e.g. Rohlf, 1994; Goree and Fuller, 1976).

The total flux threading the loop is

$$\Phi = \frac{n\hbar}{2e} \quad \text{Eq. 2}$$

cont'd. on
pg. 8...

Visiting Fellows' Reports

Some tests to characterize a magnetic transition <40K in claystones

Charles Aubourg and Myriam Kars

Université Cergy Pontoise, France
aubourg@u-cergy.fr

Pyrrhotite (Fe_7S_8), siderite (FeCO_3) and rhodochrochite (MnCO_3) have a magnetic transition at 35K, 38K and 32K respectively [1-5]. This narrow range of temperature can lead to misinterpretations and our aim, during our 10-day visit, was to perform additional tests, including RT-SIRM, ZFC, K, hysteresis loops and FORC, to better understand the <40K magnetic transitions observed commonly in claystones.

Monoclinic pyrrhotite has a ~35K crystallographic transition of unknown origin [2, 6]. For pyrrhotite minerals >1 μm , this transition is characterized by a drop of RT-SIRM and LT-SIRM [6]. Siderite and rhodochrochite have Néel magnetic transitions from a paramagnetic to antiferromagnetic state [4, 5]. In rocks, there is generally a substitution between Mn^{2+} and Fe^{2+} , resulting in a Néel temperature varying between 38K (siderite) and 32K (rhodochrochite) [5]. In siderite-bearing rocks, Housen et al. [3] observed a shift along the Y-axis of hysteresis loops for $T < 40\text{K}$ after applying a field-cooled (FC hysteresis loop). Kosterov et al. [5] observed similar shifts for rhodochrochite minerals (+Y or -Y) when measuring FC hysteresis loops measured below the Néel temperature (<40K).

Aubourg and Pozzi [7] observed a Néel-like magnetic transition at ~35K in claystones where pyrrhotite and magnetite constitute the magnetic assemblage. During the cooling of the RT-SIRM, an induced magnetization develops from ~80K parallel to the trapped magnetic field inside the MPMS [8]. Similarly, the warming of the LT-SIRM (obtained at 10K) showed a drop of one to two

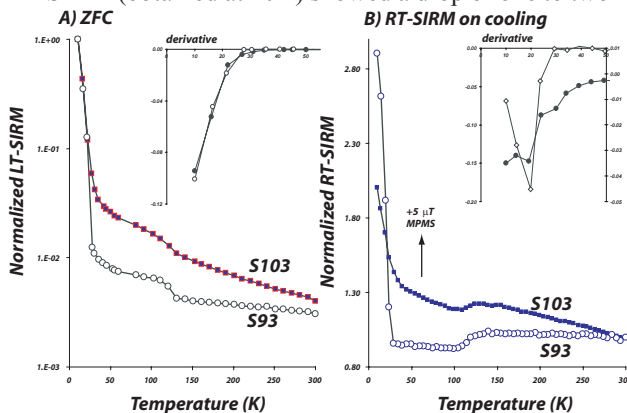


Figure 1: ZFC and RT-SIRM curves obtained from two Eocene claystones from Borneo. On cooling of RT-SIRM, we applied a magnetic field (5 μT) upward directed inside the MPMS. Both claystones show a Verwey transition, a P-transition at ~35K (sample S93 on RT-SIRM cooling curve), and a rhodochrochite -like transition at ~30K (sample S103).

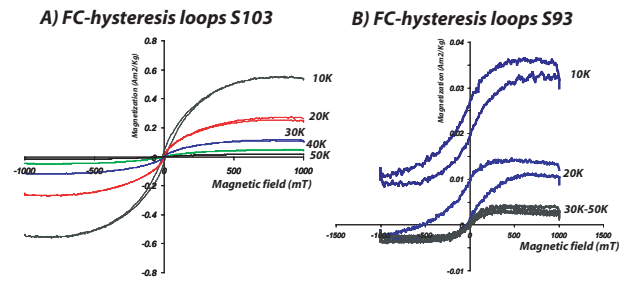


Figure 2: Hysteresis curves at low-temperature (from 50K to 10K). A field-cooled is applied during initial cooling from 300K to 10K. Note the shift of hysteresis loops for sample S103 where rhodochrochite is detected.

orders in magnitude from 10K to 50K, just like the pyrrhotite transition. Aubourg and Pozzi [8] proposed that this peculiar RT-SIRM transition, that they named the P-transition, is the signature of fine-grained pyrrhotite (<1 μm).

We show representative results obtained from two claystones from Borneo prism. The samples S93 and S103 display similar ZFC curves (Fig. 1A) resulting in comparable derivative curves (Fig. 1A, inset). As Néel-like transition is sensitive to the trapped field inside the MPMS, which is variable from one instrument to another, we applied an upward magnetic field of 5 μT during cooling of RT-SIRM (RT-SIRM is imparted at 300K with an upward magnetic field of 2.5T). The RT-SIRM curves on cooling show distinct patterns between the two samples (Fig. 1B). A P-transition is observed in sample S103. It is characterized by a regular increase of RT-SIRM from ~80K to 10K. In sample S93, we observe a sharp break-in-slope of the RT-SIRM at ~30K. The derivative curves of samples S93 and S103 precise these trends (inset, Fig. 1B). The P-transition behavior of sample S103 cannot be explained solely by the input of paramagnetic clays because the low-field magnetic susceptibility is similar for both claystones ($K=62 \mu\text{SI}$ for sample S93 and $K=87 \mu\text{SI}$ for sample S103).

We show FC hysteresis loops obtained from ~10K to ~100K after slope correction (Figure 2A). Both samples show strong paramagnetic input at room temperature (data are not shown). In sample S103, the hysteresis loops are well centered through the origin and the coercivity remains low (Fig. 2A). By contrast, for sample S93, a positive shift along the Y-axis is observed for 10K to 30K. Similarly, we note an increase of coercivity because saturation is not achieved at 1T at 10K. This +Y shift is diagnostic of siderite [3] and rhodochrochite [5]. When cooled below the Néel temperature, siderite and rhodochrochite get a strong coercive magnetization ($H_c \gg 1\text{T}$) that is not erased when running hysteresis loops.

We ran also FORC diagrams obtained at 300K, 100K and 20K (results are not shown). At 300K, these strong paramagnetic claystones S103 and S93 display the signature of low-coercive magnetic mineral, likely magnetite which is consistent with the Verwey transition observed in ZFC and RT-SIRM curves (Fig. 1). At 100K, the paramagnetic input is lower and the FORC are more representative of the magnetic assemblage. In both claystones, we see an assemblage of non-interacting magnetic

minerals in the range of coercivity from few mT up to 80 mT. This is consistent with an assemblage of magnetite and possibly pyrrhotite. At 20K, the FORC of S103 and S93 are different. The coercivity is soft for sample S103, while a stripe develops for sample S93, attesting for a distribution of a large coercivity spectrum.

We performed susceptibility measurements at different magnetic fields (from ~16 to ~240 A/m). We did not observe any field-dependency. However, the out-of-phase magnetic susceptibility (K') increases for both samples from ~40K to 5K (Fig. 3) Note that there is two orders of magnitude between K' of S103 and K' of S93. K' is larger in sample S103 where P-transition develops. There are several ways to interpret the increase of K' . One is to consider that the mineral conductivity increases significantly and that Foucault currents developed. Besnus [9], who was the first to recognize the ~35 K transition in pyrrhotite crystals, observed a large drop of resistivity from ~50K and below. It was even believed that the pyrrhotite might be a superconductor for $T < 35K$ (G. Fillion, Institut Néel, pers. com., 2008).

From this set of low-temperature measurements, we propose that magnetite and rhodochrochite constitutes the main magnetic assemblage of claystones S93. In claystones S103 where magnetite is also present, we propose that the P-transition is due to the contribution of fine-grained (<1 μm) pyrrhotite although we cannot rule out completely the input of a rhodochrochite-like Néel transition.

To distinguish between rhodochrochite-like carriers and pyrrhotite-like carriers in claystones, the ZFC curves are not adapted (Fig. 1A). RT-SIRM can help by applying a weak magnetic field (5 μT) during cooling, leading to the identification of a P-transition (Fig. 1B). FC-hysteresis loops below the Néel temperature of siderite and rhodochrochite allows identifying shifted-loops along Y-axis, which are diagnostic of siderite and rhodochrochite (Fig. 2). The identification of a sharp increase of the out-of-phase magnetic susceptibility from ~40K is diagnostic of claystones which display the P-transition (Fig. 3) and thus possibly the occurrence of ultra fine pyrrhotites.

Acknowledgments: We thank IRM for providing us

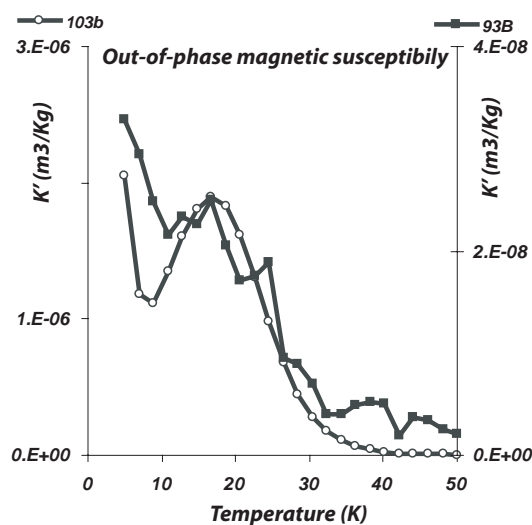


Figure 3: Out-of-phase magnetic susceptibility of samples S93 and S103. Note that the scale is two-order larger in magnitude for sample S93.

low-temperature facilities during our 10-day visit. We benefited from helpful technical assistance as well as invaluable discussion. This work is a part of M.K. PhD funded by a Cifre grant (funded by Total). F. Sapin and M. Pubellier provided us claystones from Borneo.

References

- [1] Dekkers, M.J., 1989. Magnetic properties of natural pyrrhotite part 2: high and low temperature behavior of Jrs and TRM as a fonction of grain size. *Phys. Earth Planet. Ints.*, 52: 376-393.
- [2] Rochette, P., Fillion, G., Mattéi, J.-L. and Dekkers, M.J., 1990. *Earth Planet. Sci. Lett.*, 98: 319-328.
- [3] Housen, B.A., Banerjee, S.K. and Moskowitz, B.M., 1996. *Geophys. Res. Lett.*, 23(No.20): 2843-2846.
- [4] Frederichs, T., von Dobeneck, T., Bleil, U. and Dekkers, M.J., 2003. *Phys. Chem. Earth*, 28.
- [5] Kosterov, A., Frederichs, T. and von Dobeneck, T., 2006. *Phys. Earth Planet. Int.*, 154: 234-242.
- [6] Dekkers, M.J., Mattei, J.-L., Fillion, G. and Rochette, P., 1989. *Geophys. Res. Lett.*, 16: 855-858.
- [7] Aubourg, C., and Pozzi, J.P., 2007. *IRM Quarterly*, 17(3).
- [8] Aubourg, C. and Pozzi, J.P., submitted. A new <250°C geothermometer for sedimentary rocks. *Earth Planet. Sci. Lett.*

Contribution of biogenic minerals found in ants and termites to the magnetic properties of soils

Jairo Francisco Savian

University of São Paulo, Brazil
savian@iag.usp.br

Biomineralization by social insects has been described in literature for more than two decades [1-5]. The presence of magnetite particles in migratory ants (*Pachycondyla marginata*) occurring in southeastern Brazil was reported by Acosta-Avalos et al. [6]. These ants seem to follow an approximately north-south direction during migration [7],

and they prey on live termites of the species *Neocapritermes opacus*, in which Esquivel et al. [4] and Oliveira et al. [5] also identified magnetic particles. Starting from the premise that the magnetic particles produced by these insects are released in the environment, and contribute to the magnetization of the soil, we are conducting a comparative magnetic characterization of the soil and the insects.

Soil samples were collected from two sites (samples 40 and 41) at 5m and 10m from the ant nest. At each site samples were taken at the surface and at depths of 25cm and 45cm (samples labeled a, b, and c, respectively). Two other samples (42 and 43) were collected from the termite and ant nests, respectively.

The magnetic measurements consisted of hysteresis loops (high and low-temperature), ZFC/FC curves and RTSIRM performed during my stay at IRM from 2-12

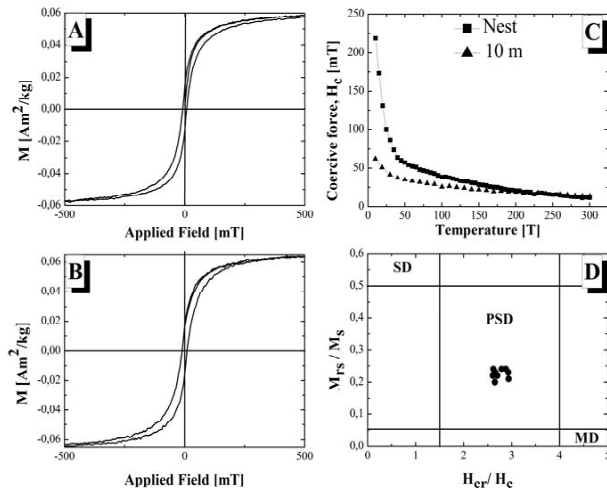


Figure 1. Hysteresis loops for (A) termite nest (JF42A) and (B) soil at 10m from the nest (JF40A); (C) Coercive force H_c versus temperature for same samples; (D) day plot for soil samples, termites and ant nests.

September, 2008. Hysteresis loops were performed at room and low-temperature for 13 samples of soil and for the insects. Maximum field of 1.5 T was applied at select temperatures from ≈ 10 K to 300 K, and measurements were made by means of a vibrating sample magnetometer (VSM) with a liquid He cryostat. Room temperature loops for the termite nest and soil samples (Figure 1) show very similar behavior. These results as well as the coercive force variation with temperature point to the presence of titanomagnetites [8, 9] as in a pseudo-single domain scale as shown by the Day plot [10].

Low-temperature remanence measurements were made from 10 K to 300 K with a Quantum Design (MPMS2) SQUID magnetometer. Samples were cooled down to 10 K in zero field, and measurements were made up to 300 K at steps of 10 K. The ZFC/FC and RTSIRM remanence curves for the termite nest sample show very similar pattern (Fig. 2A, 2C) with no Verwey transition characteristic of magnetite. The ant nest show a similar behavior (Fig.

2B, 2D). However, low temperature remanence variation curves show slight inflections between 100 K and 120 K, probably related to PSD titanomagnetite.

According to the above results all samples displayed similar behavior indicating that PSD titanomagnetite are found both in the termite nest and surrounding soil. No differences were noticed for soil samples from different depths. Results from termites (ZFC/FC, RTSIRM and hysteresis loops) are very similar to the nest and soil sample (Fig. 2E, 2G), but ants seem to display magnetic characteristics comparable with magnetite (Verwey transition at 120K) (Fig. 2F, 2H). Further interpretations are still in progress.

I would like to thank to the IRM for this opportunity, in particularly to Thelma Berquó and Mike Jackson for their assistance with the measurements, as well as all the IRM staff and students for very profitable discussions and suggestions.

References

- [1] Gould, J.L., J.L. Kirschvinck, K.S. Deffeyes, M.L. Brines, J. Exp. Bio., 86, 1-8, 1980.
- [2] Kirschvinck, J.L., D.L. Jones, and B.J. MacFadden (Eds.). Magnetite biomineralization and magnetoreception in organisms: a new biomagnetism, Plenum Press, New York, 1985.
- [3] Maher, B., Proc. R. Soc. Lond. B, 265, 733-737, 1998.
- [4] Esquivel, D.M.S., E. Wajnberg, G.R. Cernicchiaro, O.C. Alves, J. Magn. Magn. Mater. 278, 117-121, 2004.
- [5] Oliveira, J.F., E. Wajnberg, D.M.S. Esquivel, O.C. Alves, J. Magn. Magn. Mater. 294, e171-e174, 2005.
- [6] Acosta-Avalos, D., E. Wajnberg, P.S. Oliveira, I. Leal, M. Farina, D.M.S. Esquivel, J. Exp. Bio. 202, 2687-2692, 1999.
- [7] Leal, I.R. and P.S. Oliveira, Behav. Ecol. Sociobiol. 37, 373-383, 1995.
- [8] Wang, D. and R. Van der Voo, Earth Planet. Sci. Lett. 220, 175-184, 2004.
- [9] Özdemir, Ö and W. O'Reilly, Phys. Earth Planet. Inter. 25, 406-418, 1981.
- [10] Day, R., M. Fuller and V.A. Schmidt, Phys. Earth Planet. Inter. 13, 260-267, 1977.

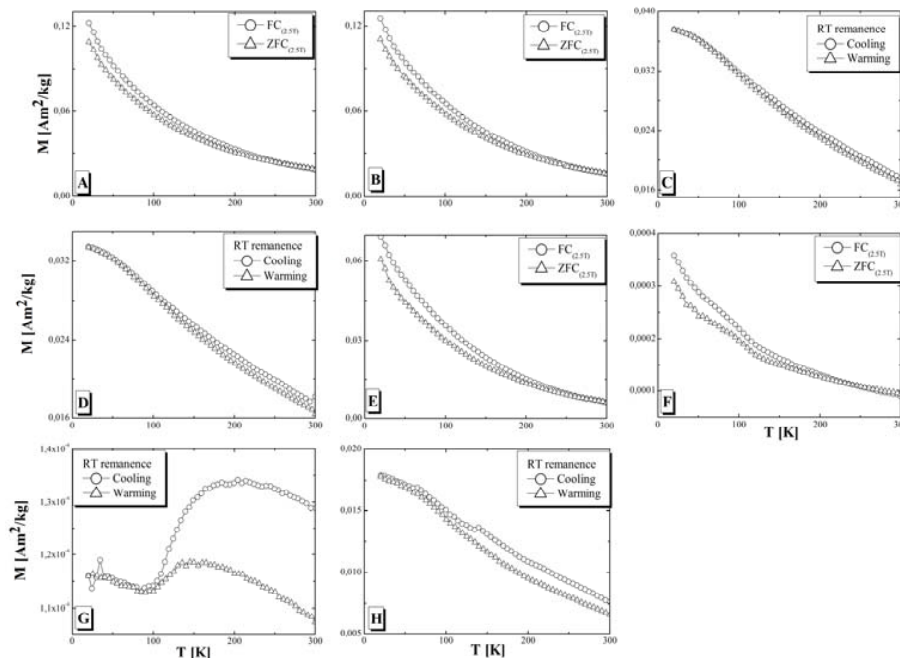


Figure 2. Low-temperature demagnetization curves of SIRM acquired at 5-300 K. FC/ZFC curves of the termite (A) and ant nests (B); RTSIRM curves for the termite (C) and ant nest (D); (E, F) ZFC/FC and RTSIRM curves for the *Neocapritermes opacus* termite (E and G, respectively) and *Pachycondyla marginata* ant (F and H, respectively).

Current Articles

A list of current research articles dealing with various topics in the physics and chemistry of magnetism is a regular feature of the IRM Quarterly. Articles published in familiar geology and geophysics journals are included; special emphasis is given to current articles from physics, chemistry, and materials-science journals. Most abstracts are taken from INSPEC (© Institution of Electrical Engineers), Geophysical Abstracts in Press (© American Geophysical Union), and The Earth and Planetary Express (© Elsevier Science Publishers, B.V.), after which they are subjected to Procrustean culling for this newsletter. An extensive reference list of articles (primarily about rock magnetism, the physics and chemistry of magnetism, and some paleomagnetism) is continually updated at the IRM. This list, with more than 10,000 references, is available free of charge. Your contributions both to the list and to the Abstracts section of the IRM Quarterly are always welcome.

Anisotropy

- Caballero-Miranda, C.I., J.R. Torres-Hernandez, and L.M. Alva-Valdivia, Anisotropy of magnetic susceptibility analysis of the Cantera Ignimbrite, San Luis Potosi, Mexico: flow source recognition, *Earth Planets Space*, 61 (1), 173-182, 2009.
- Essalhi, M., S. Sizaret, L. Barbanson, Y. Chen, Y. Branquet, D. Panis, P. Camps, P. Rochette, and A. Canals, Track of fluid paleocirculation in dolomite host rock at regional scale by the Anisotropy of Magnetic Susceptibility (AMS): An example from Aptian carbonates of La Florida, Northern Spain, *Earth Planet. Sci. Lett.*, 277 (3-4), 501-513, 2009.
- Oliva-Urcia, B., J.C. Larrasoana, E.L. Pueyo, A. Gil, P. Mata, J.M. Pares, A.M. Schleicher, and O. Pueyo, Disentangling magnetic subfabrics and their link to deformation processes in cleaved sedimentary rocks from the Internal Sierras (west central Pyrenees, Spain), *J. Struct. Geol.*, 31, 163-176, 2009.
- Petronis, M., and J. Geissman, Anisotropy of magnetic susceptibility data bearing on the transport direction of mid-tertiary regional ignimbrites, Candelaria Hills area, West-Central Nevada, *B. Volcanol.*, 71 (2), 121-151, 2009.
- Shumway, J.R., and N.R. Iverson, Magnetic fabrics of the Douglas Till of the Superior lobe: exploring bed-deformation kinematics, *Quat. Sci. Rev.*, 28 (1-2), 107-119, 2009.

Archeomagnetism

- Hartmann, G.A., R.I.F. Trindade, A. Goguitchaichvili, C. Etchevarne, J. Morales, and M.C. Afonso, First archeointensity results from Portuguese potteries (1550-1750 AD), *Earth Planets Space*, 61 (1), 93-100, 2009.
- Lopez-Tellez, J.M., B. Aguilar-Reyes, J. Morales, A. Goguitchaichvili, M. Calvo-Rathert, and J. Urrutia-Fucugauchi, Magnetic characteristics and archeointensity determination on Mesoamerican Pre-Columbian Pottery from Quiahuitlan, Veracruz, Mexico, *Geofisica Internacional*, 47, 329-340, 2008.
- Morales, J., A. Goguitchaichvili, G. Acosta, T. Gonzales-Moran, L. Alva-Valdivia, J. Robles-Camacho, and M. Hernandez-Bernal, Magnetic properties and archeointensity determination on Pre-Columbian pottery from Chiapas, Mesoamerica, *Earth Planets Space*, 61, 83-91, 2009.
- Pavón-Carrasco, F.J., M.L. Osete, J.M. Torta, and L.R. Gaya-Piqué, A regional archeomagnetic model for Europe for the last 3000 years, SCHA.DIF.3K: Applications to archeomagnetic dating, *Geochem. Geophys. Geosyst.*, 10, 2009.

- Di Vito, M.A., E. Zanella, L. Gurioli, et al., The Afragola settlement near Vesuvius, Italy: The destruction and abandonment of a Bronze Age village revealed by archaeology, volcanology, and rock-magnetism, *Earth Planet. Sci. Lett.*, 277, 408-421, 2009.
- Feinberg, J.M., P.R. Renne, J. Arroyo-Cabrales, M.R. Waters, P. Ochoa-Castillo, and M. Perez-Campa, Age constraints on alleged "footprints" preserved in the Xalnene Tuff near Puebla, Mexico, *Geology*, 37 (3), 267-270, 2009.
- Lodge, A., and R. Holme, Towards a New Approach to Archaeomagnetic Dating in Europe Using Geomagnetic Field Modelling, *Archaeometry*, 51, 309-322, 2009.

Bio(geo)magnetism

- Carvalho, C., S. Hickey, D. Faivre, N. Menguy, Formation of magnetite in *Magnetospirillum gryphiswaldense* studied with FORC diagrams, *Earth Planets Space*, 61, 143-150, 2009.
- Keim, C.N., U. Lins, and M. Farina, Manganese in biogenic magnetite crystals from magnetotactic bacteria, *Fems Microbiology Letters*, 292 (2), 250-253, 2009.
- Langley, S., P. Igric, Y. Takahashi, Y. Sakai, D. Fortin, M.D. Hannington, and U. Schwarz-Schampera, Preliminary characterization and biological reduction of putative biogenic iron oxides (BIOS) from the Tonga-Kermadec Arc, southwest Pacific Ocean, *Geobiology*, 7 (1), 35-49, 2009.
- Fuentes-Farias, A.L., J. Urrutia-Fucugauchi, G. Gutierrez-Ospina, L. Perez-Cruz, and V.H. Garduno-Monroy, Magnetic features of marine black turtle natal beaches and implications for nest selection, *Geofisica Internacional*, 47, 311-318, 2008.
- Li, J.H., Y.X. Pan, G.J. Chen, Q.S. Liu, L.X. Tian, and W. Lin, Magnetite magnetosome and fragmental chain formation of *Magnetospirillum magneticum* AMB-1: transmission electron microscopy and magnetic observations, *Geophys. J. Int.*, 177 (1), 33-42, 2009.

Environmental Magnetism and Paleoclimate

- Hannam, J.A., and J.A. Dearing, Mapping soil magnetic properties in Bosnia and Herzegovina for landmine clearance operations, *Earth Planet. Sci. Lett.*, 274, 285-294, 2008.
- Heil, C.W.J., J.G. Rosenbaum, R.L. Reynolds, and S.M. Colman, Paleomagnetism and environmental magnetism of GLAD800 sediment cores from Bear Lake, Utah and Idaho, in *Paleoenvironments of Bear Lake, Utah and Idaho, and its catchment: Geological Society of America Special Paper 450*, edited by J.G. Rosenbaum, and D.S. Kaufman, pp. 291-310, 2009.
- Itambi, A.C., T. von Dobeneck, S. Mulitza, T. Bickert, and D. Heslop, Millennial-scale northwest African droughts related to Heinrich events and Dansgaard-Oeschger cycles: Evidence in marine sediments from offshore Senegal, *Paleoceanography*, 24, 2009.
- Kohler, C.M., D. Heslop, M.J. Dekkers, W. Krijgsman, D.J.J. van Hinsbergen, and T. von Dobeneck, Tracking provenance change during the late Miocene in the eastern Mediterranean using geochemical and environmental magnetic parameters, *Geochem. Geophys. Geosys.*, 9, 2008.
- Nelson, F.E., R. Barendregt, and M. Villeneuve, Stratigraphy of the Fort Selkirk Volcanogenic Complex in central Yukon and its paleoclimatic significance: Ar/Ar and paleomagnetic data, *Can. J. Earth Sci.*, 46, 381-401, 2009.
- Rosenbaum, J.G., W.E. Dean, R.L. Reynolds, and M.C. Reheis, Alloctenic sedimentary components of Bear Lake, Utah and Idaho, in *Paleoenvironments of Bear Lake, Utah and Idaho, and its catchment: Geological Society of America Special*

- Paper 450, edited by J.G. Rosenbaum, and D.S. Kaufman, 148-168, 2009.
- Rosenbaum, J.G., and C.W.J. Heil, The glacial/deglacial history of sedimentation in Bear Lake, Utah and Idaho., in *Paleoenvironments of Bear Lake, Utah and Idaho, and its catchment: Geological Society of America Special Paper 450*, edited by J.G. Rosenbaum, and D.S. Kaufman, pp. 247-261, 2009.
- Smith, M.L., B.J. Pillans, and K.G. McQueen, Paleomagnetic evidence for periods of intense oxidative weathering, McKinnons mine, Cobar, New South Wales, *Aust. J. Earth Sci.*, 56 (2), 201-212, 2009.
- Villasante-Marcos, V., C.J. Hollis, G.R. Dickens, and M.J. Nicolo, Rock magnetic properties across the Paleocene-Eocene Thermal Maximum in Marlborough, New Zealand, *Geologica Acta*, 7 (1-2), 229-242, 2009.
- Zawadzki, J.Ç., T. Magiera, P. Fabijańczyk, Geostatistical evaluation of magnetic indicators of forest soil contamination with heavy metals, *Stud. Geophys. Geod.*, 53, 133-149, 2009.

Geomagnetism

- Harrison, C.G.A., Latitudinal signature of Earth's magnetic field variation over the last 5 million years, *Geochem. Geophys. Geosys.*, 10, 2009.
- Lawrence, K.P., L. Tauxe, H. Staudigel, C.G. Constable, A. Koppers, W. McIntosh, and C.L. Johnson, Paleomagnetic field properties at high southern latitude, *Geochem. Geophys. Geosys.*, 10, 2009.
- Leonhardt, R., K. Fabian, M. Winklhofer, A. Ferk, C. Laj, and C. Kissel, Geomagnetic field evolution during the Laschamp excursion, *Earth Planet. Sci. Lett.*, 278 (1-2), 87-95, 2009.
- Mazaud, A., J.E.T. Channell, C. Xuan, and J.S. Stoner, Upper and lower Jaramillo polarity transitions recorded in IODP Expedition 303 North Atlantic sediments: Implications for transitional field geometry, *Phys. Earth Planet. Int.* 172 (3-4), 131-140, 2009.
- Quidelleur, X., J. Carlut, P. Tchilinguirian, A. Germa, P.Y. Gillot, Paleomagnetic directions from mid-latitude sites in the southern hemisphere (Argentina): Contribution to time averaged field models, *Phys. Earth Planet. Int.* 172, 199-209, 2009.
- Valet, J.P., G. Plenier, and E. Herrero-Bervera, Geomagnetic excursions reflect an aborted polarity state, *Earth Planet. Sci. Lett.*, 274 (3-4), 472-478, 2008.
- Brandt, D., G.A. Hartmann, E. Yokoyama, E.L. Catelani, and R.I.F. Trindade, Paleointensity data from Early Cretaceous Ponta Grossa dikes (Brazil) using a multisample method, *Earth Planets Space*, 61, 41-49, 2009.
- Brown, M.C., M.N. Graton, J. Shaw, R. Holme, and V. Soler, Microwave palaeointensity results from the Matuyama-Brunhes geomagnetic field reversal, *Phys. Earth Planet. Int.*, 173 (1-2), 75-102, 2009.
- Calvo-Rathert, M., A. Goguitchaichvili, and N. Vegas-Tubia, A paleointensity study on middle Miocene to Pliocene volcanic rocks from south-eastern Spain, *Earth Planets Space*, 61 (1), 61-69, 2009.
- Gogorza, C.S.G., S. Torcida, M.A. Irurzun, M.A.E. Chaparro, and A.M. Sinito, Application of the pseudo-Thellier technique to a paleomagnetic record from lake El Trebol (Patagonia, Argentina), *Geofisica Internacional*, 47 (4), 319-327, 2008.
- Goguitchaichvili, A., R. Cejudo Ruiz, L. Sanchez Bettucci, B. Aguilar Reyes, L.M. Alva-Valdivia, J. Urrutia-Fucugauchi, J. Morales, and M. Calvo Rathert, New absolute paleointensity results from the Parana Magmatic Province (Uruguay) and the Early Cretaceous geomagnetic paleofield, *Geochem. Geophys. Geosyst.*, 9, 2008.
- Goguitchaichvili, A., M.A. Cervantes, M.C. Rathert, P. Camps, J. Sologashvili, and G. Maissuradze, Gilbert-Gauss geomagnetic reversal recorded in Pliocene volcanic sequences from Georgia (Lesser Caucasus): revisited, *Earth Planets Space*, 61 (1), 71-81, 2009.
- Nachasova, I., and K. Burakov, Determination of the ancient geomagnetic field elements from thermal remanent magnetization corrected for magnetic anisotropy, *Izvestiya-Phys. Solid Earth*, 45 (1), 41-46, 2009.
- Ohno, M., F. Murakami, F. Komatsu, Y. Guyodo, G. Acton, T. Kanamatsu, H.F. Evans, and F. Nanayama, Paleomagnetic directions of the Gauss-Matuyama polarity transition recorded in drift sediments (IODP Site U1314) in the North Atlantic, *Earth Planets Space*, 60 (12), E13-E16, 2008.
- Selkin, P.A., J.S. Gee, W.P. Meurer, and S.R. Hemming, Paleointensity record from the 2.7 Ga Stillwater Complex, Montana, *Geochem. Geophys. Geosys.*, 9, 2008.
- Shcherbakova, V.V., M. Perrin, V.P. Shcherbakov, V.E. Pavlov, A. Ayz'yan, and G.V. Zhidkov, Rock magnetic and paleointensity results from Mesozoic baked contacts of Armenia, *Earth Planets Space*, 61 (1), 23-39, 2009.
- Tanaka, H., N. Komuro, and G.M. Turner, Palaeosecular variation for 0.1-21 Ka from the Okataina Volcanic Centre, New Zealand, *Earth Planets Space*, 61 (1), 213-225, 2009.

Instrumentation and Techniques

- Durr, H.A., T. Eimuller, H.J. Elmers, et al., A Closer Look Into Magnetism: Opportunities With Synchrotron Radiation, *IEEE Trans. Magnetics*, 45, 15-57, 2009.
- Ionita, V., and E. Cazacu, Magnetic Hysteresis Modelling Based on Magneto-Optical Kerr Effect, *Revue Roumaine Des Sciences Techniques-Serie Electrotechnique Et Energetique*, 53, 455-462, 2008.
- Poidras, T., P. Camps, and P. Nicol, Controlled atmosphere vibrating thermo-magnetometer (CatVTM): a new device to optimize the absolute paleointensity determinations, *Earth Planets Space*, 61 (1), 101-110, 2009.

Magnetic Field Records/Paleointensity

- Biggin, A.J., G. Strik, and C.G. Langereis, The intensity of the geomagnetic field in the late-Archaeon: new measurements and an analysis of the updated IAGA palaeointensity database, *Earth Planets Space*, 61 (1), 9-22, 2009.

Mineral and Rock Magnetism

- Afremov, L., V. Belokon, and K. Nefedev, Magnetic aftereffect in systems of single-domain interacting particles and magnetic viscosity of rocks, *Izvestiya-Phys. Solid Earth*, 45 (1), 57-62, 2009.
- Alva-Valdivia, L.M., M. Perrin, M.L. Rivas-Sanchez, A. Goguitchaichvili, H. Lopez-Loera, O.F. Lopes, and T.B. Bonas, Rock magnetism and microscopy of the Jacupiranga alkaline-carbonatitic complex, southern Brazil, *Earth Planets Space*, 61 (1), 161-171, 2009.
- Chang, L., A.P. Roberts, C.J. Rowan, Y. Tang, P. Pruner, Q.W. Chen, C.S. Horng, Low-temperature magnetic properties of greigite (Fe₃S₄), *Geochem. Geophys. Geosys.*, 10, 2009.
- Dillon, M., and C. Franke, Diagenetic alteration of natural Fe-Ti oxides identified by energy dispersive spectroscopy and low-temperature magnetic remanence and hysteresis measurements, *Phys. Earth Planet. Int.* 172 (3-4), 141-156, 2009.
- Harrison, R.J., Magnetic ordering in the ilmenite-hematite solid

Free the Flux! (What is “Trapped Flux”?)

You may have come across the phrase “trapped flux” in reference to a SQUID magnetometer. What exactly is trapped flux and how do you get rid of it? The simplest example of trapped flux comes from cooling a superconducting ring in the presence of a magnetic field. Once the ring is below the critical temperature, any attempt to remove the field will generate a persistent current in the ring that opposes the change. The flux threading the loop will therefore remain constant, even if the external field is removed. i.e. -- you have trapped flux. The only way to untrap it is to heat the ring above its critical temperature and set the flux free.

solution: A computational study of the low-temperature spin glass region, *Geochem. Geophys. Geosyst.*, 10, 2009.

- Kasama, T., R.E. Dunin-Borkowski, T. Asaka, R.J. Harrison, R.K.K. Chong, S.A. McEnroe, E.T. Simpson, Y. Matsui, and A. Putnis, The application of Lorentz transmission electron microscopy to the study of lamellar magnetism in hematite-ilmenite, *Am. Mineral.*, 94 (2-3), 262-269, 2009.
- Kosterov, A., G. Conte, A. Goguitchaichvili, and J. Urrutia-Fucugauchi, Low-temperature magnetic properties of andesitic rocks from Popocatepetl stratovolcano, Mexico, *Earth Planets Space*, 61 (1), 133-142, 2009.
- Kosterov, A., and K. Fabian, Twinning control of magnetic properties of multidomain magnetite below the Verwey transition revealed by measurements on individual particles, *Geophys. J. Int.*, 174 (1), 93-106, 2008.
- Lee, S.J., H. Jung, S. Lee, and J. Dho, Superparamagnetic behaviour of reentrant weak-ferromagnetic phase in haematite crystal at low temperatures, *New J. Phys.*, 11, 2009.
- Liu, Q.S., T. Yang, Q.L. Zeng, J.P. Zheng, Y.H. Luo, N. Qiu, H.J. Xu, and Z.M. Jin, Magnetic study of the UHP eclogites from the Chinese Continental Scientific Drilling (CCSD) Project, *J. Geophys. Res.*, 114, 2009.
- Muxworthy, A.R., D. Heslop, and D.M. Michalk, Thermal fluctuation fields in basalts, *Earth Planets and Space*, 61 (1), 111-117, 2009.
- O’Driscoll, B., and M.S. Petronis, Oxide mineral formation during the serpentinization of a Cr-spinel seam: Insights from rock magnetic experiments, *Geochem. Geophys. Geosys.*, 10, 2009.
- Ozdemir, O., D.J. Dunlop, and M. Jackson, Frequency and field dependent susceptibility of magnetite at low temperature, *Earth Planets Space*, 61 (1), 125-131, 2009.
- Perrin, M., A. Saleh, and L. Alva-Valdivia, Cenozoic and Mesozoic basalts from Egypt: a preliminary survey with a view to paleointensity, *Earth Planets Space*, 61 (1), 51-60, 2009.
- Smirnov, A.V., Grain size dependence of low-temperature remanent magnetization in natural and synthetic magnetite: Experimental study, *Earth Planets Space*, 61, 119-124, 2009.

Mineral Physics and Chemistry

- Bosi, F., U. Halenius, H. Skogby, Crystal chemistry of the magnetite-ulvospinel series, *Am. Mineral.*, 94, 181-189, 2009.
- Clayton, K.E., J.R. Koby, and J.A. TenCate, Limitations of Preisach Theory: Elastic aftereffect, congruence, and end point memory, *Geophys. Res. Lett.*, 36, 2009.

- Coffey, W.T., P.M. DeJardin, Y.P. Kalmykov, Reversal time of magnetization of single-domain ferromagnetic particles with mixed uniaxial - cubic anisotropy, *Phys. Rev. B*, 79, 2009.
- Ito, E., H. Fukui, T. Katsura, et al., Determination of high-pressure phase equilibria of Fe₂O₃ using the Kawai-type apparatus equipped with sintered diamond anvils, *Am. Mineral.*, 94 (2-3), 205-209, 2009.

Tectonics/Paleomagnetism

- Borradaile, G.J., and I. Geneviciene, Late Proterozoic reconstructions of North-West Scotland and Central Canada: Magnetic fabrics, paleomagnetism and tectonics, *J. Struct. Geol.*, 30 (12), 1466-1488, 2008.
- Brandt, D., M. Ernesto, A.C. Rocha-Campos, and P.R. dos Santos, Paleomagnetism of the Santa Fe Group, central Brazil: Implications for the late Paleozoic apparent polar wander path for South America, *J. Geophys. Res.*, 114, 2009.
- Goguitchaichvili, A., A. Pozzo, J.L. Rocha-Fernandez, J. Urrutia-Fucugauchi, and A.M. Soler-Arechalde, Paleomagnetic and rock-magnetic study on volcanic units of the Valsequillo Basin: implications for early human occupation in central Mexico, *Earth Planets Space*, 61 (1), 205-211, 2009.
- Jay, A.E., C. Mac Niocaill, M. Widdowson, S. Self, and W. Turner, New palaeomagnetic data from the Mahabaleshwar Plateau, Deccan Flood Basalt Province, India: implications for the volcanostratigraphic architecture of continental flood basalt provinces, *J. Geol. Soc. London*, 166, 13-24, 2009.
- Kodama, K.P., Simplification of the anisotropy-based inclination correction technique for magnetite- and haematite-bearing rocks: a case study for the Carboniferous Glenshaw and Mauch Chunk Formations, North America, *Geophys. J. Int.*, 176, 467-477, 2009.
- Levashova, N.M., R. Van der Voo, A.V. Abrajevitch, M.L. Bazhenov, Paleomagnetism of mid-Paleozoic subduction-related volcanics from Chingiz Range in NE Kazakhstan: The evolving paleogeography of amalgamating Eurasian composite continent, *Geol. Soc. Am. Bull.*, 121, 555-573, 2009.
- Meert, J.G., F.D. Pruet, E. Merino, An “Inverse Conglomerate” Paleomagnetic Test and Timing of In Situ Terra Rossa Formation at Bloomington, Indiana, *J. Geol.*, 117, 126-138, 2009.
- Piper, J.D.A., Uplift and cooling magnetisation record in the Bamble and Telemark terranes, Sveconorwegian orogenic belt, SE Norway, and the Grenville-Sveconorwegian loop, *Tectonophysics*, 463 (1-4), 185-207, 2009.
- Sbarbori, E., L. Tauxe, A. Goguitchaichvili, J. Urrutia-Fucugauchi, and W.A. Bohron, Paleomagnetic behavior of volcanic rocks from Isla Socorro, Mexico, *Earth Planets Space*, 61 (1), 191-204, 2009.

Other

- Casas, L., and A. Incoronato, Application of the relocation-error distribution on geomagnetic databases. Analyses on the “Historical Italian Geomagnetic Data Catalogue”, *Ann. Geophys.*, 51, 553-562, 2008.
- Gurarii, G., and M. Aleksyutin, Wavelet analysis of paleomagnetic data: 2. How irregular sedimentation rate and breaks in the studied section affect the results, *Izvestiya-Phys. Solid Earth*, 45, 21-30, 2009.
- Saracco, G., N. Thouveny, D.L. Bourles, and J.T. Carcaillet, Extraction of non-continuous orbital frequencies from noisy insolation data and from palaeoproxy records of geomagnetic intensity using the phase of continuous wavelet transforms, *Geophys. J. Int.*, 176 (3), 767-781, 2009.

SQUIDS, continued from pg. 1

and the fundamental flux quantum is therefore

$$\Phi_0 = \frac{\hbar}{2e} \approx 2 \times 10^{-15} \text{ Wb} \quad \text{Eq. 3}$$

where \hbar is Planck's constant ($h/2\pi$), e is the charge on an electron, and the factor of two accounts for the fact that the electrons travel in Cooper pairs.

To envision how flux quantization and superconductivity could allow us to measure magnetic fields, imagine a superconducting ring in the presence of a steadily increasing flux (Fig. 2). As the external flux (Φ_E) increases, a persistent (super)current is induced in the loop. (Because current flows without resistance, it will persist until the external flux changes.) The current in turn induces a flux (Φ_I) inside the loop that is equal and opposite to Φ_E . The total flux inside the loop (Φ_T) remains constant (at zero Φ_0) and is the sum of the external flux and that generated by the current in the loop. When the critical current is reached (in this example at a flux of $0.75 \Phi_0$), the loop is no longer superconducting and a flux quantum can enter the loop. The quantum state of the loop has now changed by $+1$, and the total flux inside the loop is $1 \Phi_0$. This requires the current to reverse direction so that $\Phi_E + \Phi_I = 0.75 + 0.25 = 1 \Phi_0$. As the external flux continues to increase, the current decreases (and then increases again in the opposite direction) so that the flux inside the loop remains at $1 \Phi_0$. When I_c is again reached, the loop reverts to its normal state and another flux quantum enters. The step-wise nature of the flux increases in the ring makes them easy to count, and in theory, by monitoring the current and the number of times it makes discrete jumps, one could precisely measure both flux quanta and fractions of flux quanta.

In practice, the above-described flux switching device is not very sensitive. The size of the loop is constrained by thermal energy considerations to be so small that sensitivity would be very limited. Additionally, the field required to exceed the critical current is large enough that the device operates ineffectually (Goree and Fuller, 1976). A number of applications allow for more sensitive flux switching, and the Josephson junction is perhaps the most important.

The Josephson Effect and Josephson Junction.

Brian Josephson predicted in 1962 that supercurrent will flow between two superconductors separated by an insulator. Although the original Josephson junction consisted of an insulating layer separating two superconductors, similar behavior is observed with any kind of weak link between two superconductors. Other types of junctions include a thin oxide layer, a narrow constriction, a superconducting point contact, or a normal (non-superconducting) metal sandwich junction (Gallop and Petley, 1976; Petley, 1980). (See back cover for an example junction.)

We can understand this Josephson effect if we remember that all Cooper pairs in a superconductor have the same quantum-mechanical wave function. If the insulator is narrow enough, the waves on either side of the insulating junction overlap, allowing the Cooper pairs to “tunnel”

through the insulator. The critical current across such a junction is much less than in a true superconductor, so that in a superconducting ring containing a Josephson junction, flux switching will occur at smaller applied field increments.

The current flowing across the junction is a function of the phase difference (δ) between the two superconductors on either side of the insulator:

$$I = I_c \sin(\delta), \quad \text{Eq. 4}$$

where I_c is the critical current of the junction. Equation 4 is known as the DC Josephson effect. There are many other fascinating phenomena associated with tunneling behavior and Josephson junctions in presence of current and magnetic flux, but in the interest of simplicity, we will rudely overlook them for now.

When a weak link or Josephson junction is inserted in a superconducting ring, the requirement that the total phase difference around the loop be $2\pi n$ (Eq. 1) still holds and takes the form:

$$\delta + 2\pi \frac{\Phi_T}{\Phi_0} = 2\pi n \quad \text{Eq. 5}$$

where $2\pi\Phi_T/\Phi_0$ is the phase difference due to the flux threading the loop. It follows that flux threading a loop is no longer precisely quantized (Petley, 1980), i.e. Φ_T/Φ_0 can take on fractional values because of the phase difference across the junction.

Putting it all together

There are two ways in which the Josephson junction is typically used to measure magnetic flux: the single-junction (RF) SQUID and the double-junction (DC) SQUID.

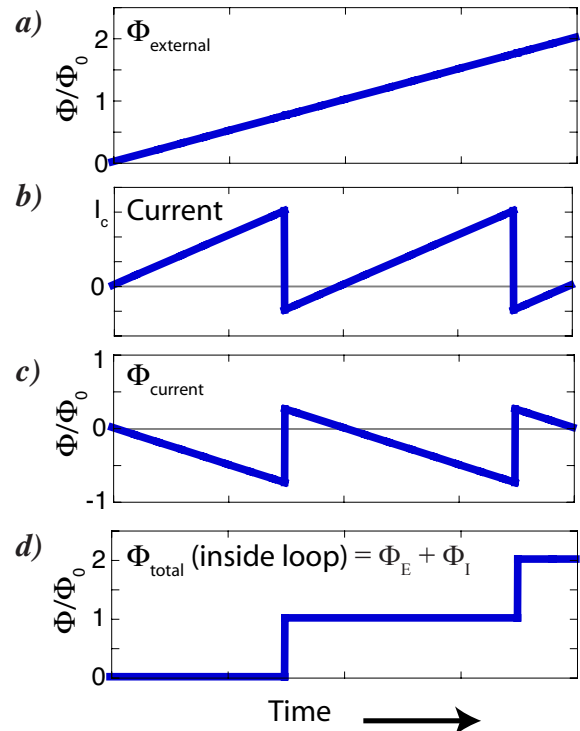


Figure 2. In the presence of a steadily increasing external field (a), the current in a superconducting ring is generated (b), which in turn induces an equal and opposite flux (c). The total flux inside the loop is quantized (d). In this example, the critical current of the ring is reached at $\Phi = 0.75\Phi_0$.

The DC SQUID has considerably higher precision and was developed first, but for many years was not in common use because of the high cost of manufacturing the junctions. Now that junction fabrication is far less costly, most new instruments use the DC SQUID. Simplified descriptions of DC and RF SQUIDS are given below and draw heavily on Clarke (1993), Braginski and Clarke (2004), and Bruynseraede et al (1993).

The Double Junction (DC) SQUID. The DC SQUID consists of two identical Josephson junctions arranged in parallel on a superconducting loop (Fig. 3a). Each junction has a critical current I_0 , and a DC bias current (I_B) is applied to the device. In the absence of any applied (external) flux (and for $I_B < 2I_0$), the current flowing across each junction is $I_B/2$. The critical current for the entire device (I_C) is $2I_0$, at which point both junctions revert to the normal state simultaneously. Additionally, the phase change across the entire device (δ) should be independent of the path traveled and thus equal to the phase change across each junction: $\delta = \delta_1 = \delta_2$.

In the presence of increasing external (sample) flux (Φ_E), a circulating current is induced in the ring (I_Φ) to counter the applied flux. This current adds to the bias cur-

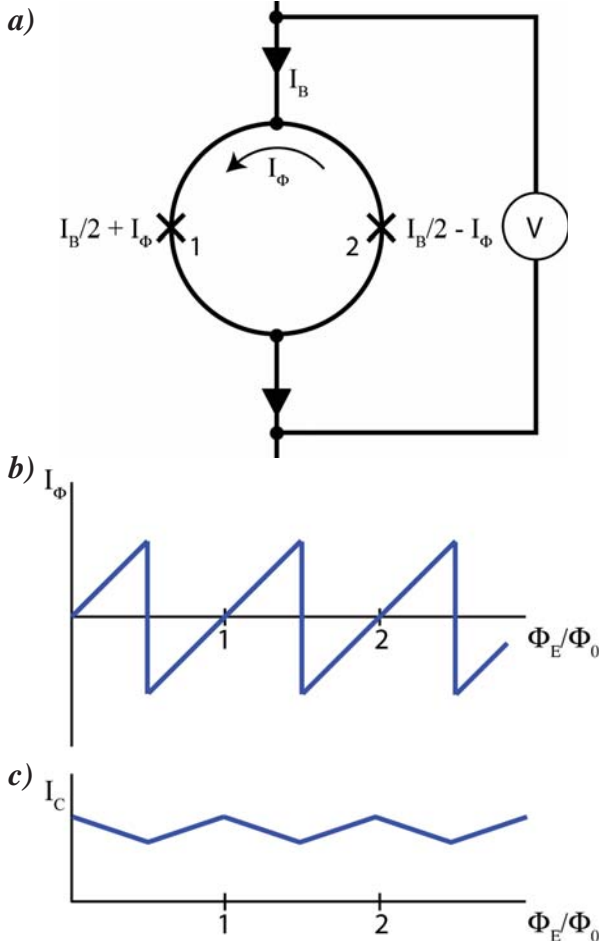


Figure 3. (a) Schematic representation of a DC SQUID. Two Josephson junctions (X) are arranged in parallel on a superconducting ring. The device is biased with a DC current (I_B), and voltage (V) is measured across the SQUID. (b) Induced circulating current (I_Φ) in the ring is a function of applied flux, and (c) interference between the two junctions causes the critical current (I_C) of the device to vary periodically with applied flux. (After Clarke, 1993)

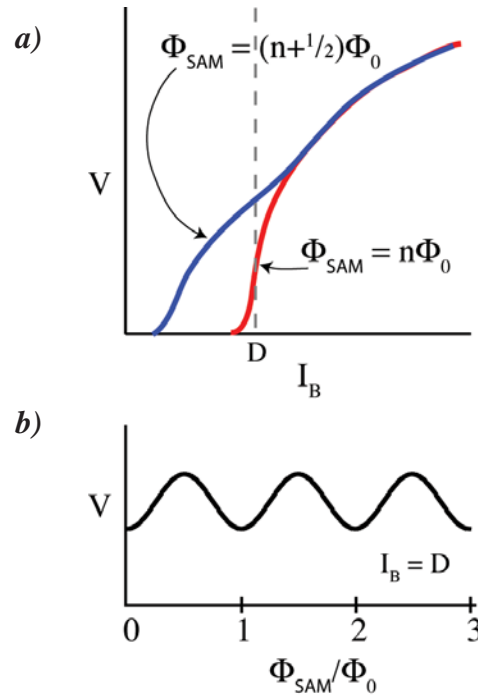


Figure 4. (a) Voltage as a function of bias current for DC SQUID. (b) Voltage as a function of sample flux for constant bias current (e.g. point D in (a)). (After Clarke, 1993)

rent in junction 1 ($I_1 = I_B/2 + I_\Phi$) and subtracts from the bias current in junction 2 ($I_2 = I_B/2 - I_\Phi$). Now, junction 1 will reach its critical current before junction 2 (when $I_B/2 + I_\Phi = I_0$); when this happens, the device reverts to the normal state, a flux quantum enters the ring, and the circulating current reverses direction (Fig. 3b). The limiting critical current for the entire device is therefore $I_C = 2I_0 - 2I_\Phi$ and varies periodically with applied flux (Fig. 3c) as the two junctions interfere with each other. This **interference** is analogous to that generated by optical waves in a double slit experiment; in this case a single quantum-mechanical wave is “split” by the junctions into two waves that interfere with each other so as to modulate the critical current of the device.

Slightly more formally, the total current across the device is the sum of the current across each junction:

$I_B = I_1 + I_2$, and by Equation 4, the current across each junction is a function of the phase change across the junction:

$$I_B = I_0 \sin(\delta_1) + I_0 \sin(\delta_2) \quad \text{Eq. 6}$$

In the absence of any flux, $\delta_1 = \delta_2 = \delta$ (above), and therefore $I_1 = I_2$. In the presence of flux threading the loop, the total phase change around the loop is given by Equation 5, and the phase change across each junction (in the direction of I_B) is:

$$\delta_1 = \delta + \pi\Phi_T/\Phi_0 \quad \text{Eq. 7}$$

$$\delta_2 = \delta - \pi\Phi_T/\Phi_0 \quad \text{Eq. 8}$$

The total current across the device is therefore:

$$I = I_0 \sin\left(\delta + \frac{\pi\Phi_T}{\Phi_0}\right) + I_0 \sin\left(\delta - \frac{\pi\Phi_T}{\Phi_0}\right) \quad \text{Eq. 9}$$

or
$$I = 2I_0 \sin(\delta) \cos\left(\frac{\pi\Phi_T}{\Phi_0}\right) \quad \text{Eq. 10}$$

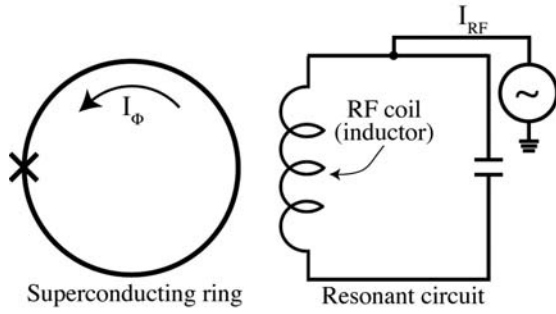


Figure 5. Schematic representation of an RF SQUID. A superconducting ring with a single Josephson junction (X) is inductively coupled to a resonant circuit which induces an alternating flux on the ring. The ring's response is a function of the applied field, and a voltage that is periodic with applied (sample) flux is generated in the resonant circuit. (After Clarke, 1993, and Braginski & Clarke, 2004)

The maximum supercurrent, or critical current, is achieved when $\sin(\delta) = 1$, so

$$I_C = 2I_0 \cos\left(\frac{\pi\Phi_T}{\Phi_0}\right) \quad \text{Eq. 11}$$

In practice, the DC SQUID is operated at a bias current that is greater than I_C (e.g. point D in Fig. 4a). In this mode, a voltage develops across the device (Fig. 4a) that is a function of both I_B and Φ_E (or Φ_{SAM} when the external flux results from a sample approaching the SQUID). Voltage is at a maximum where I_C is minimized at $(n+1/2)\Phi_0$, and V is at a minimum where I_C is maximized ($n\Phi_0$). Because I_C varies with applied flux (Fig. 3c), at constant I_B output voltage also varies periodically with the applied flux (Fig. 4b).

The Single Junction (RF) SQUID. The RF SQUID consists of a superconducting loop of inductance L containing a single junction. The operation of this device is more difficult to understand intuitively, but we start by noting that the RF SQUID is not technically a SQUID; with only one junction, it does not operate using the interference phenomenon described above for the DC SQUID. In the RF SQUID, the loop is inductively coupled to a resonant circuit¹, which is driven at (or near) its resonant frequency by the current I_{RF} (Fig. 5). A voltage across the resonant circuit provides the device output.

The current flowing across the junction (and around the ring) is easily derived from Equations 4 and 5 and is $-I_C \sin(2\pi\Phi_T/\Phi_0)$. The resulting relationship between applied (external) flux (Φ_E) and flux inside the ring (Φ_T) is shown in Figure 6 (for the most commonly-used case where $2\pi LI_c \geq \Phi$). The external flux is the sum of an alternating flux generated by the resonant circuit/RF coil (Φ_{RF}), and a quasi-static flux from the sample being measured (Φ_{SAM}).

For the moment, let us ignore the sample contribution and consider the operation of the device only in the presence of the RF field ($\Phi_E = \Phi_{RF}$). This function is repre-

sented by the thin gray dashed curve in Figure 6a. Only the positively sloping segments are stable, because when the alternating external flux is large enough to cause $I_\Phi > I_C$, flux will enter or exit the ring, and the device will trace out the path indicated by the heavy, solid (red) lines.

The peak output voltage ($V_{RF,max}$) measured across the resonant circuit is a function both of the RF drive current and of the sample flux (Fig. 6b). Let us continue to consider the case where $\Phi_{SAM} = 0$. For small values of I_{RF} , not enough flux is generated to cause the SQUID to exceed its critical current, and it remains in the “zero” quantum state, tracing a path back and forth along a portion of line segment ae (Fig. 6a). Until I_{RF} reaches A , $V_{RF,max}$ increases linearly with I_{RF} (Fig. 6b). When the drive current reaches A , the applied flux is sufficient to cause the SQUID to exceed I_C , it temporarily admits a quantum of flux, and follows the path $abcd$ or $efgh$ (Fig. 6a). This transition causes energy to dissipate in the resonant circuit, meaning that the peak induced flux on the next half-cycle will be less than that required to reach the ab or ef transition, even though I_{RF} remains at A . The device will stay in the initial (quantum) state on path ae , building up energy over

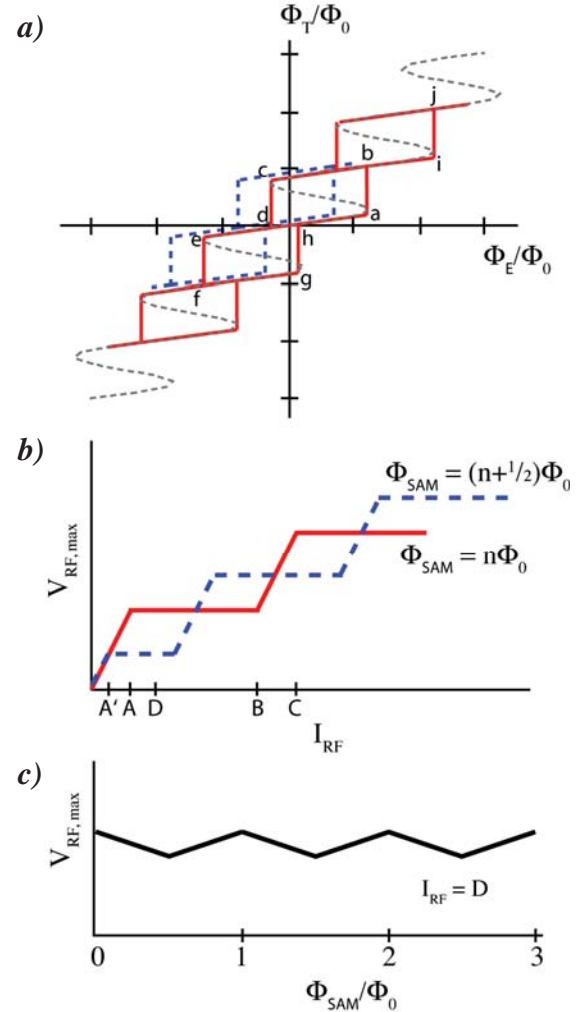


Figure 6. (a) Relationship between external and internal flux in an RF SQUID (gray dashed line). Solid red line shows stable response in the absence of any sample flux. Dashed blue line shows stable response in the presence of $0.5 \Phi_0$ quasi-static sample flux. (b) Peak voltage achieved across the resonant circuit as a function of RF drive current. (c) At constant drive current, voltage as a function of applied (sample) flux. (After Clarke, 1993)

¹ A resonant circuit consists of a capacitor (C) connected to an inductor (L). Current can alternate between the two at the circuit's resonant frequency. The circuit is also known as an LC circuit, or a tank circuit because the oscillating behavior of the current is similar to water sloshing back and forth in a tank.

the course of many RF cycles. Eventually, Φ_{RF} will be sufficient to make the ab or ef transition again, and the process will be repeated. As I_{RF} is increased beyond A , the quantum transitions (ab or ef) still occur at the same voltage, but this peak voltage is achieved more frequently. When the drive current reaches point B , each cycle of the RF causes the SQUID to execute a complete double-hysteresis loop ($abcdefgh$), and further increases in I_{RF} now cause an increase in the measured peak voltage (Fig. 6b). At $I_{RF} = C$, there is sufficient flux to exceed I_C twice, admitting two flux quanta (ab and ij), and so on.

The relationship between I_{RF} and $V_{RF,max}$ varies depending on the sample flux; for $\Phi_{SAM} = n\Phi_0$, the relationship is as shown by the solid (red) line. For $\Phi_{SAM} = (n + 1/2)\Phi_0$, the curves shown in Figure 5a are shifted by $\Phi_0/2$ (heavy, dashed blue line), and the transition to a higher flux state (ab) can occur at a lower drive current (A'). I_{RF} is usually chosen to maximize the voltage change with change in Φ_{SAM} , and the device is operated at this constant I_{RF} (point D in Fig. 6b). $V_{RF,max}$ then varies with applied field (Φ_{SAM}), generating the output signal (Fig. 6c).

The relatively simple DC and RF devices described above become more complicated in actual operation. For example, because the SQUID itself is quite small (less than a few mm), it is typically inductively coupled to a larger-diameter superconducting pick-up coil, which provides a larger signal. Other efforts to increase the signal to noise ratio, practically measure the device output, account for hysteretic current-voltage behavior in the Josephson junctions, and many other considerations are beyond the scope of this short article. However, we will finish up by exploring one of these issues.

The Flux Locked Loop (FLL) and the Dreaded Flux Jump (DFJ). Because the applied flux to voltage relationships (Figs. 4b and 6c) are sinusoidal – especially for DC SQUIDs – the output response is non-linear for all but the smallest variations in Φ_E . To resolve this problem,

Brian David Josephson

b. 4 January, 1940, Cardiff, Wales, United Kingdom

Brian Josephson started at Cambridge University as an undergraduate, where he published his first paper reconciling differing measurements of gravitational red shift by calculating a thermal correction to the Mossbauer effect. He continued his studies at Cambridge, receiving a Masters and then a Ph.D. in Physics in 1964. Josephson is probably best known for his theoretical work on tunnel barriers in superconductors. This work was largely carried out as a graduate student and won him the Nobel Prize in Physics in 1973, which he shared with Leo Esaki and Ivar Giaever. The Josephson junctions which grew out of this work allow modern SQUID magnetometers to operate with extremely high sensitivity. Josephson moved briefly to the United States to work as a Research Assistant Professor at the University of Illinois before returning to Cambridge in 1967 to serve as Assistant Research Director of the Cavendish Laboratory. Now retired as Professor of Physics and member of the Theory of Condensed Matter Group, Josephson continues working as Director of the Mind-Matter Unification Project at the Cavendish Laboratory.

the SQUID is usually operated in a **flux-locked loop (FLL)**, or at constant flux. A feedback loop applies a flux to the SQUID that is equal and opposite to that generated by a sample. This both linearizes the output signal, and greatly increases the dynamic range of the SQUID. The feedback range is generally set to $\pm 1\Phi_0$, and each time the range is exceeded, the feedback is reset to zero and a flux quantum is counted. In this way, there is both a digital and an analog part to the signal: the number of flux quanta counted and the voltage representation of a fraction of a flux quantum, respectively.

The dreaded **flux jump** occurs when the FLL temporarily loses its lock and then recovers at a different quantum level (Foley et al., 2004). In other words, it miscounts the number of flux quanta. This typically occurs when the rate of flux change is too great, and a user will observe it when moving a strongly-magnetic sample into or out of the SQUID measurement region too quickly.

And so ends our whirlwind tour of SQUIDS. Hopefully the next time you use one, you will have a little better appreciation for what's going on behind the curtain. And if you are still a little bit baffled, draw some comfort from Aslamazov and Varlamov (2001), who note in a discussion of SQUIDS, that "...superconductivity is a complicated quantum effect. Those who want really to comprehend it have a long and hard way ahead of them. It demands many years of resolute but rewarding work." Or, if you don't have that much time, come visit the IRM during the Minnesota State Fair, where you can surely get deep-fried SQUID on a stick -- less useful, but perhaps more satisfying.

References:

- Aslamazov, L.G., and A.A. Varlamov, *The Wonders of Physics*, World Scientific, River Edge, NJ, 233 pp., 2001.
- Bardeen, J., L.N. Cooper, J.R. Schrieffer, Theory of Superconductivity, *Phys. Rev.*, 108, 1175-1204, 1957.
- Braginski, A., and J. Clarke, Introduction to *The SQUID Handbook*, v. 1, J. Clarke, and A.I. Braginski, Eds., Wiley-VCH Verlag GmbH & Co., Weinheim, 251-355, 2004.
- Bruynseraede, Y., C. Vlekken, C. Van Haesendonck, V.V. Moshchalkov, Fundamentals of Giaever and Josephson Tunneling, in *The New Superconducting Electronics*, H. Weinstock and R.W. Ralston, Eds., NATO ASI Series, 251, 123-180, 1993.
- Clarke, J., SQUIDS: Theory and practice, in *The New Superconducting Electronics*, H. Weinstock and R.W. Ralston, Eds., NATO ASI Series, 251, 123-180, 1993.
- Clarke, J., SQUIDS, *Sci. Am.*, 271, 46-53, 1994.
- Foley, C.P., M.N. Keene, H.J.M. ter Brake, and J. Vrba, SQUID system issues, in *The SQUID Handbook*, v. 1, J. Clarke, and A.I. Braginski, Eds., Wiley-VCH Verlag GmbH & Co., Weinheim, 251-355, 2004.
- Gallop, J.C., and B.W. Petley, SQUIDS and their applications, *J. Phys. E.: Sci. Instrum.*, 9, 417-429, 1976.
- Goree, W.S., and M. Fuller, Magnetometers using RF-driven Squids and their applications in rock magnetism and paleomagnetism, *Rev. Geophys. Space Phys.*, 14, 591-608, 1976.
- Josephson, B.D., Possible new effects in superconductive tunneling, *Phys. Lett.*, 1, 251, 1962.
- Kleiner, R., and D. Koelle, Basic properties of superconductivity, in *The SQUID Handbook*, v. 1, J. Clarke, and A.I. Braginski, Eds., Wiley-VCH Verlag GmbH & Co., Weinheim, 357-366, 2004.
- Petley, B.W., The ubiquitous SQUID, *Contemp. Phys.*, 21, 607-630, 1980.
- Rohlf, J.W., *Modern Physics: from α to Z^0* , John Wiley and Sons, Hoboken, NJ, 646 pp., 2004.

University of Minnesota
291 Shepherd Laboratories
100 Union Street S. E.
Minneapolis, MN 55455-0128
phone: (612) 624-5274
fax: (612) 625-7502
e-mail: irm@umn.edu
www.irm.umn.edu

Nonprofit Org.
U.S Postage
PAID
Mpls., MN
Permit No. 155

The IRM Quarterly

The *Institute for Rock Magnetism* is dedicated to providing state-of-the-art facilities and technical expertise free of charge to any interested researcher who applies and is accepted as a Visiting Fellow. Short proposals are accepted semi-annually in spring and fall for work to be done in a 10-day period during the following half year. Shorter, less formal visits are arranged on an individual basis through the Facilities Manager.

The *IRM* staff consists of **Subir Banerjee**, Professor/Founding Director; **Bruce Moskowitz**, Professor/Director; **Joshua Feinberg**, Assistant Professor/Associate Director; **Jim Marvin**, Emeritus Scientist; **Mike Jackson**, **Peat Solheid**, and **Julie Bowles**, Staff Scientists.

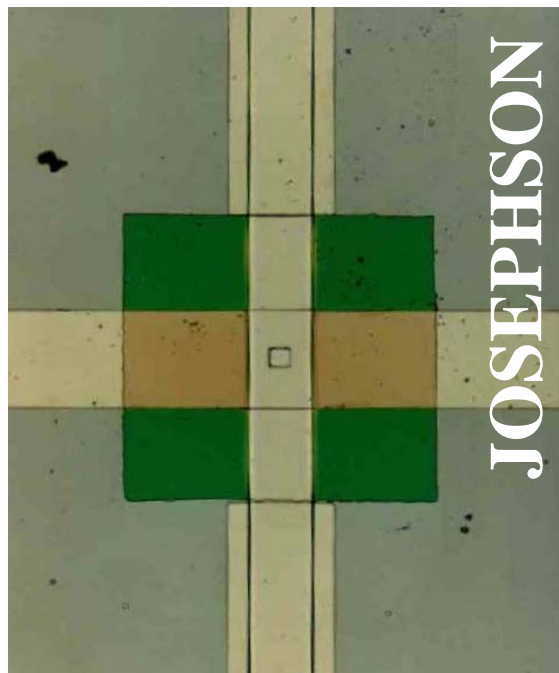
Funding for the *IRM* is provided by the **National Science Foundation**, the **W. M. Keck Foundation**, and the **University of Minnesota**.

The *IRM Quarterly* is published four times a year by the staff of the *IRM*. If you or someone you know would like to be on our mailing list, if you have something you would like to contribute (e.g., titles plus abstracts of papers in press), or if you have any suggestions to improve the newsletter, please notify the editor:

Julie Bowles
Institute for Rock Magnetism
University of Minnesota
291 Shepherd Laboratories
100 Union Street S. E.
Minneapolis, MN 55455-0128
phone: (612) 624-5049
fax: (612) 625-7502
e-mail: jbowles@umn.edu
www.irm.umn.edu

The U of M is committed to the policy that all people shall have equal access to its programs, facilities, and employment without regard to race, religion, color, sex, national origin, handicap, age, veteran status, or sexual orientation.

Right: Example of a Josephson junction



UNIVERSITY OF MINNESOTA

